Materials Research Bulletin 83 (2016) 360–368

Contents lists available at ScienceDirect

Materials Research Bulletin

journal homepage: www.elsevier.com/locate/matresbu

Visible-light-absorbing Evonik P-25 nanoparticles modified with tungstophosphoric acid and their photocatalytic activity on different wavelengths

J.A. Rengifo-Herrera[a,*], M.N. Blanco[a], M.M. Fidalgo de Cortalezzi[b,c], L.R. Pizzio[a,*]

[a] Centro de Investigación y Desarrollo en Ciencias Aplicadas "Dr. J.J. Ronco" (CINDECA), Departamento de Química, Facultad de Ciencias Exactas UNLP-CCT, La Plata, CONICET, 47 No 257, 1900, La Plata, Buenos Aires, Argentina
[b] Departamento de Ingeniería Química, Instituto Tecnológico de Buenos Aires-ITBA, Madero 399, Ciudad Autónoma de Buenos Aires, Argentina
[c] Department of Civil and Environmental Engineering, University of Missouri, Columbia, MO, USA

ARTICLE INFO

Article history:
Received 4 March 2016
Received in revised form 8 June 2016
Accepted 15 June 2016
Available online 16 June 2016

Keywords:
A. Semiconductors
B. Optical properties
C. Electron microscopy
C. Nuclear magnetic resonance (NMR)
C. Raman spectroscopy

ABSTRACT

For the first time, Evonik P-25 nanoparticles were impregnated with tungstophosphoric acid (TPA) (30% w/w) and annealed at two different temperatures, 200 °C (P25-TPA-200) and 500 °C (P25-TPA-500) for 1 h. Samples were characterized by different analytical techniques. Their photocatalytic activity was evaluated in the degradation of malachite green (MG) solutions at pH 5.0 upon three different irradiations: $\lambda_1 > 320$ nm, $\lambda_2 > 450$ nm and $\lambda_3 > 590$ nm. Only sample P25-TPA-500 showed visible-light absorption. This absorption could be related to the formation of a surface complex TPA Keggin anion-TiO_2. P25-TPA-500 and P25-TPA-200 samples showed an important dark adsorption of MG dye (~30%); however, sample P25-TPA-500 exhibited the highest photocatalytic activity either under irradiation λ_1 or λ_2. The presence of *tert*-butyl alcohol (TBA), an •OH scavenger affected the photocatalytic reaction upon irradiation λ_1, but just slightly upon irradiation λ_2. Finally, P25-TPA-200 exhibited a higher leaching of TPA than P25-TPA-500 samples.

1. Introduction

Evonik P-25, which is a mixture of anatase–rutile crystalline structures, is the commercial TiO_2 powder with highest photocatalytic activity and it is the one most widely used as standard photocatalyst. Its high photocatalytic activity has frequently been linked to low e^-/h^+ recombination since photo-produced electrons in the anatase phase can be transferred to lower energy rutile electron-trapping sites [1]. Moreover, many studies have proposed that anatase and rutile crystallites are interwoven, facilitating an efficient electron transfer at the anatase/rutile interface. Moreover, electrons may be transferred from the rutile phase to anatase surface trapping sites [2].

In spite of its high photocatalytic activity, TiO_2 Evonik P-25 absorbs only UV-A light, which corresponds to 4%–7% of the total solar irradiation hitting the planet's surface, limiting its use in solar-energy-driven applications where TiO_2 materials may absorb visible light also (~50% of total solar irradiation on the earth surface). Several approaches such as metal doping [3], non-metallic doping [3–6] and ultrasound treatment [7] have been studied in the literature to expand the light absorption of Evonik P-25 towards the visible region.

Recently, the addition of polyoxometallates (POMs), which are clusters of transition metals and oxygen often used as catalysts in thermal catalytic reactions, onto TiO_2 has risen as a promising alternative to prepare TiO_2 with visible light absorption and high photocatalytic activity [8–12]. Some studies have suggested that polyoxometallates such as tungstophosphoric acid ($H_3PW_{12}O_{40}$) and tungstosilicic acid ($H_4SiW_{12}O_{40}$) added to sol-gel synthesized TiO_2 might lead to the formation of a surface complex between the POM and TiO_2 [13], P-doping [8] or composite formation [9], all of them responsible for its visible light absorption. However, so far there are no studies reporting the modification of Evonik P-25 nanoparticles with POM.

Herein, the impregnation of Evonik P-25 nanoparticles with tungstophosphoric acid (TPA at 30% w/w) annealed at two different temperatures, 200 and 500 °C, is explored for the first time. These materials were characterized by multi-techniques using FT-Raman, UV–vis DRS, ^{31}P MAS NMR, EDX-SEM, isoelectric

* Corresponding authors.
E-mail addresses: julianregifo@quimica.unlp.edu.ar (J.A. Rengifo-Herrera), lrpizzio@quimica.unlp.edu.ar (L.R. Pizzio).

http://dx.doi.org/10.1016/j.materresbull.2016.06.026
0025-5408/

point, and potentiometric acidity. Their photocatalytic activity was evaluated in the degradation of aqueous malachite green solutions under three different irradiations: λ_1, using a cut-off filter at $\lambda > 320$ nm, λ_2 with a cut-off filter at $\lambda > 455$ nm and $\lambda 3$ with a cut-off filter at $\lambda > 590$ nm. Experiments with an •OH radical scavenger such as *tert*-butyl alcohol were also performed.

2. Materials and methods

2.1. Impregnation of tungstophosphoric acid on Evonik P-25 nanoparticles

First, 2.4 g of tungstophosphoric acid (TPA) ($H_3PW_{12}O_{40}$ 23 H_2O, Fluka, corresponding to 1.83 g of tungsten) was dissolved in 50 mL of a solution (70% absolute ethanol, 30% distilled water) at pH 1.5 (by adding HCl) in order to avoid the partial degradation of TPA Keggin anion. Then, 4 g of Evonik P-25 nanoparticles was added to reach a TPA concentration of 30% (w/w). This suspension was left until the solvent was completely dried. The solid was washed three times with distilled water in order to remove weakly bonded TPA, and the aqueous residues were evaluated by atomic absorption spectrometry in order to determine the tungsten content in the solid. These results revealed that most part of tungsten (1.79 g from the 1.83 g initially added) remains in TiO_2. Finally, the solid was annealed at 200 and 500 °C for 1 h under air atmosphere, obtaining the samples named P25-TPA-200 and P25-TPA-500, respectively.

2.2. Sample characterization

2.2.1. Scanning electron microscopy with energy dispersive X-ray spectroscopy (SEM-EDX)

The secondary electron micrographs of the samples were obtained by scanning electron microscopy (SEM) using Phillips 505 Model equipment and EDAX 9100 analyser at a working potential of 15 kV and graphite-supported samples metallized with gold.

2.2.2. Diffuse reflectance spectroscopy (DRS)

The diffuse reflectance spectra of samples were recorded using a UV–vis Lambda 35, Perkin-Elmer spectrophotometer equipped with a diffuse reflectance chamber Labsphere RSA-PE-20 which contains an integrating sphere of 50 mm diameter and internal Spectralon coating is attached, in the 250–800 nm wavelength range.

2.2.3. Fourier transform Raman spectroscopy (FT-Raman)

Raman scattering spectra were recorded on a Raman Horiba-Jobin-Yvon T64000 instrument with an Ar+ laser source of 488 nm wavelength in a macroscopic configuration.

2.2.4. Nuclear magnetic resonance spectroscopy (NMR)

The ^{31}P magic angle spinning-nuclear magnetic resonance (^{31}P MAS NMR) spectra were recorded on Bruker Avance II equipment, using the CPA/MAS ^{1}H-^{31}P technique. A sample holder 4 mm in diameter and 10 mm in height was employed, using 5 ms pulses, a repetition time of 4 s, and working at a frequency of 121.496 MHz for ^{31}P at room temperature. The spin rate was 8 KHz, and several hundred pulse responses were collected. Phosphoric acid 85% was used as external reference.

2.2.5. Acidity measurements by potentiometric titration

The acidity of the solid samples was measured by means of potentiometric titration. The solid (0.05 g) was suspended in acetonitrile (Merck) and stirred for 3 h. Then, the suspension was titrated with 0.05 N *n*-butylamine (Carlo Erba) in acetonitrile, using Metrohm 794 Basic Titrino apparatus with a double junction electrode.

2.2.6. Isoelectric point (IP)

The isoelectric point was calculated from zeta potential measurements at different pH values. Laser Doppler velocimetry was applied to characterize the electrophoretic mobility (EPM) of the particles using a Malvern Zetasizer Nano ZS. Measured EPMs were converted to zeta potential using the Smoluchowski equation:

$$U = \varepsilon\zeta/\mu$$

where U is the electrophoretic mobility, ε is the dielectric constant of the solution, μ is its viscosity, and ζ is the zeta potential.

Disposable folded capillary cells were employed. Initially, 0.05 g of solid was suspended in 15 mL of Milli-Q water, and the solution pH was modified by adding HCl or NaOH.

2.2.7. Atomic absorption spectrometry (AAS)

Tungsten (W) determination was carried out using an atomic absorption spectrophotometer Varian AA model 240. The calibration method was used with standards prepared in the laboratory. Analyses were carried out at a wavelength of 254.9 nm; bandwidth, 0.3 nm; lamp current, 15 mA; phototube amplification, 800 mV; burner height, 4 mm; and acetylene-nitrous oxide flame (11:4).

2.2.8. Photocatalytic activity

The photocatalytic activity was evaluated using a 300 W Xe-Arc lamp (Newport, USA) as light source, which emits an estimated average irradiance of 3.6 mW m^{-2} nm^{-1} in the range 380–430 nm. This system was equipped with glass cut-off filters (Newport, USA): irradiation λ_1: cut-off filter $\lambda > 320$ nm, irradiation λ_2: cut-off filter $\lambda > 450$ nm, and irradiation λ_3: cut-off filter $\lambda > 590$ nm. Lamp emission spectrum and transmittance of cut-off filters are available in supplementary material (Fig. S1).

Malachite green (MG) (Sigma-Aldrich) solutions 1×10^{-5} M were used as organic target. First, 0.05 g of photocatalyst was added to 50 mL of MG solutions with initial pH 5.0 in a 100 mL Pyrex bottle and kept in the dark under constant stirring for 30 min in order to ensure that MG/TiO_2 adsorption/desorption equilibrium was reached. Then, suspensions were illuminated with irradiation λ_1, λ_2 or λ_3 for 60 min. Samples were taken at different irradiation times, and the discoloration of MG solutions was followed using a Perkin-Elmer Lambda 35 spectrophotometer at 618 nm. All experiments were carried out in triplicate, and an average was calculated, obtaining standard deviations below 8%.

Leaching experiments were performed in the absence of malachite green by adding 0.05 g of sample to 50 mL of distilled water, which was irradiated with irradiation λ_1, for 2 h. The solid was separated by centrifugation and the supernatant was analysed by AAS.

3. Results

3.1. Characterization of Degussa P-25 nanoparticles modified with TPA

SEM micrographs (Fig. 1) revealed that Evonik P-25 consists of small particles and agglomerates. It is well known that Evonik P-25 consists of nanoparticles and agglomerates with an average diameter of 20 nm and 1 μm, respectively [1,14]. Furthermore, EDX measurements revealed the presence of Ti and O on the surface. On the other hand, SEM images of TPA-impregnated P-25 TiO_2 samples exhibited a size increase in the agglomerates when the annealing temperature rose from 200 to 500 °C. The EDX measurements revealed the existence of W Lα1 and Mα1 signals at 8.396 and 1.779 KeV, respectively, in P25-TPA samples. They do not overlap the Au Mα1 signal at 2.126 eV which comes from the sample metallization process.

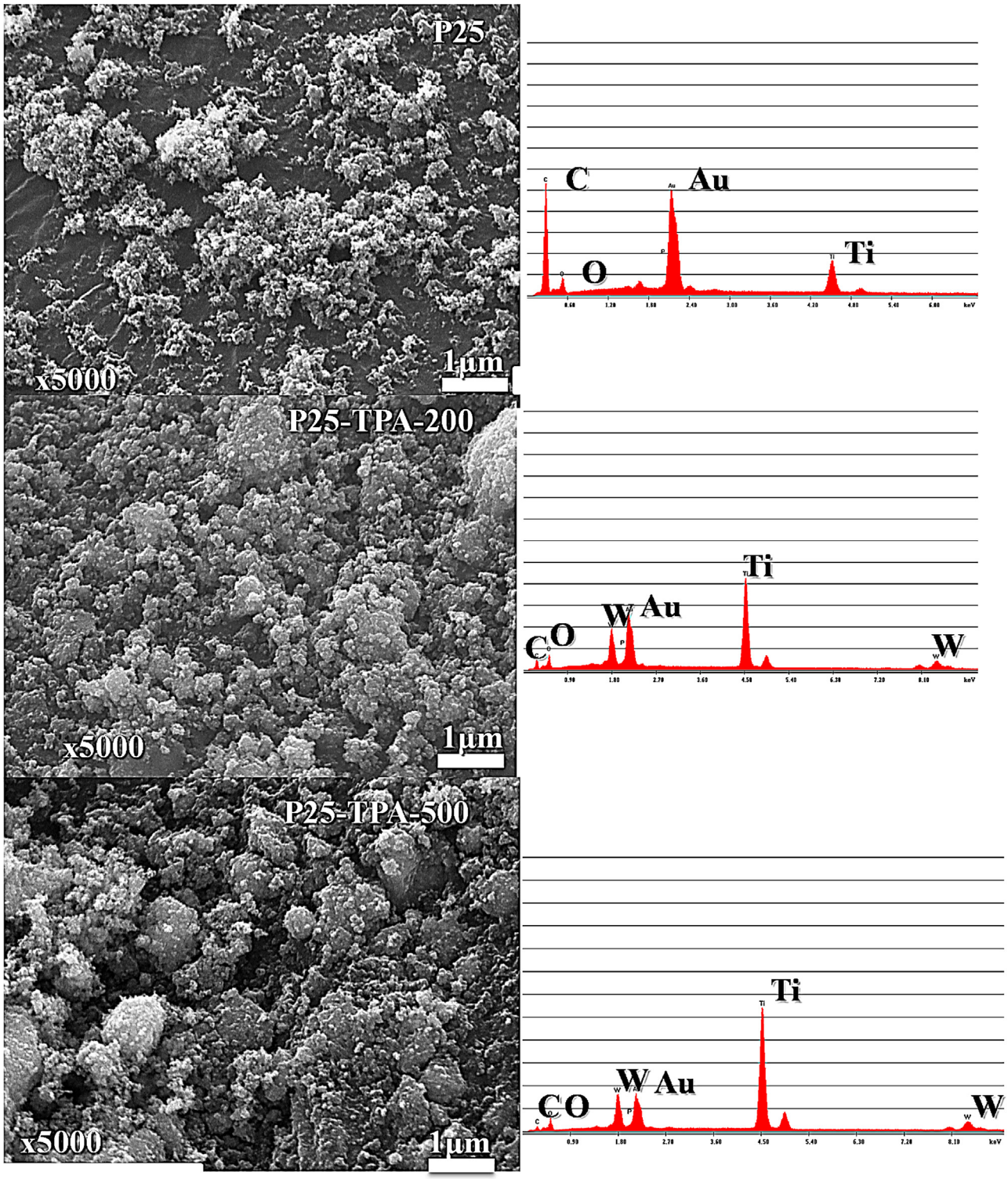

Fig. 1. SEM micrographs and EDX measurements of Degussa P-25, P25-TPA-200 and P25-TPA-500 samples.

Fig. 2 shows the light-harvesting ability of all samples. Evonik-P25 and P25-TPA-200 samples present the typical light absorption of anatase or rutile nanoparticles in the UV region ($\lambda < 400$ nm), attributed to electron transitions from the valence band to the conduction band [1,14]. However, in addition to the UV absorption due to TiO_2, the P25-TPA-500 sample presented an interesting absorption in the blue region of the spectra between 400 and 500 nm. Impregnated TPA samples of TiO_2 P25 did not show any absorption features related to bulk TPA.

The Raman spectra of bulk TPA, P25-TPA-200, P25-TPA-500 and non-annealed P25-TPA (P25-TPA-NA) samples are shown in Fig. 3. The spectrum of bulk TPA exhibited Raman bands at 1080, 990, 930 and 890 cm^{-1} corresponding to the asymmetric vibrations of P—O, W=O, W—O—W bonds in the Keggin anion [15,16]. In the P25-

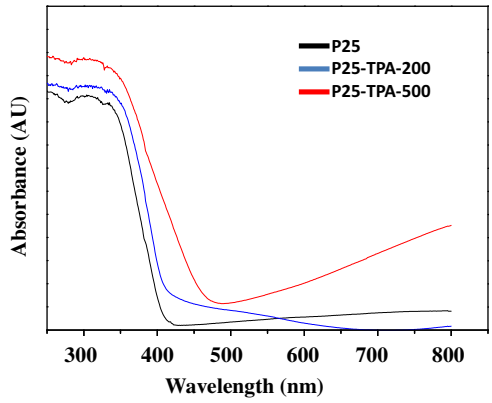

Fig. 2. DRS UV–vis spectra of samples.

TPA-NA sample, the anatase phase peaks at 141, 394, 514 cm^{-1} are observed, which agrees well with Raman vibrations of anatase TiO_2 indicating that it is the predominant crystalline structure in TiO_2 P25 (Fig. 3a) [17]. Moreover, in this sample, two intense bands also appeared at 987 and 1028 cm^{-1}, which are attributed to the presence of the Keggin anion of TPA (Fig. 3b). The P25-TPA-200 sample showed the same Raman characteristics of either TiO_2 or TPA, except for a slight blue shift of the most intense Raman band attributed to Ti—O bonds of anatase TiO_2 that shifts from 141 cm^{-1} to 144 cm^{-1} (Fig. 3c). Fig. 3c shows that the P25-TPA-500 sample underwent a strong blue shift of Ti—O Raman band (148 cm^{-1}) and moreover, this sample exhibited a broad shoulder between 950 and 1000 cm^{-1} (Fig. 3b).

The ^{31}P MAS NMR spectra are shown in Fig. 4. In the literature, it is reported that bulk hydrated TPA exhibits only one peak at about −15 ppm with a small linewidth [18]. Herein, bulk TPA was annealed at two temperatures, 200 and 500 °C, in order to study the effect of temperature on TPA stability and its ^{31}P signal. Bulk TPA dehydrated at 200 °C exhibits a narrow peak at −15.3 ppm, which matches very well the hydrated TPA peak. At 500 °C, there is a broader main peak at −13.2 ppm and a shoulder at −15.5 ppm. The former could be assigned to dimeric anion ($[P_2W_{21}O_{71}]^{6-}$) and the latter to Keggin anion [13,15].

Regarding TPA impregnated on TiO_2 Evonik P25, the sample annealed at 200 °C shows a narrow peak localized at −15.4 ppm corresponding a Keggin anion, while the sample annealed at 500 °C exhibits a broader main peak at −14.6 ppm with an important shoulder at ca. −11.2 ppm.

Acid strength measurements by potentiometric titration with *n*-butylamine were also carried out on the samples (Fig. 5). The initial electrode potential (E_i) indicates the maximum acid strength of the sites and the value of meq amine g^{-1} solid where the plateau is reached indicates the total number of acid sites. Thus, the acid strength of these sites can be classified according to the following scale: Ei > 100 mV (very strong sites), $0 < E_i < 100$ mV (strong sites), $-100\ mV < E_i < 0$ (weak sites), $E_i < -100$ mV (very weak sites) [19,20].

Often, anatase and rutile nanoparticles show an acid strength around $E_i = 100$ mV due to the presence of terminal and bridge Ti—OH groups on the surface [21]. Bulk TPA ($H_3PW_{12}O_{40}$) exhibited a higher acid strength ($E_i = 800$ mV) due to the presence of 3 very acid protons. However, this parameter increased for P25 impregnated samples. P25-TPA-NA and P25-TPA-200 samples showed stronger acid strength ($E_i = 450$ mV) than P25-TPA-500 ($E_i = 393$ mV).

The isoelectric point (IP) of Evonik-P-5 (Table 1) matches very well those from anatase TiO_2 (IP = 6.0). The samples P25-TPA-200 and P25-TPA-500 exhibited acid IPs (1.4 and 2.0, respectively), which indicates the presence of acid sites on the TiO_2 surface.

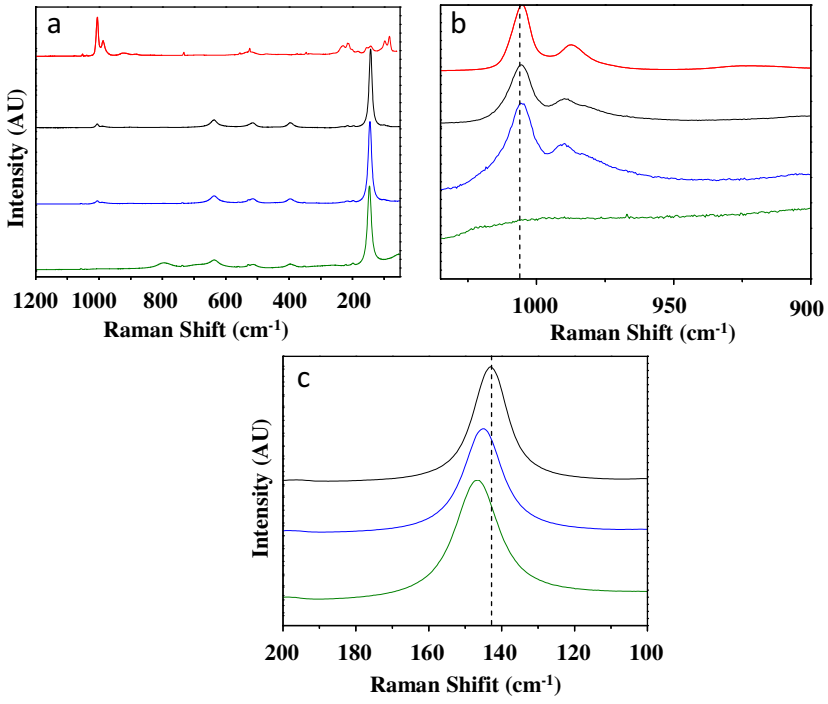

Fig. 3. FT-Raman spectra of samples. (▬) Bulk TPA, (—) P-25-TPA-NA, (▬) P25-TPA-200, (▬) P25-TPA-500.

Table 1
Isoelectric point of samples.

Sample	Isoelectric point (IP)
Evonik-P-25	5.8
P25-TPA-200	1.6
P25-TPA-500	2.0

3.2. Photocatalytic activity of samples under UV and visible irradiation

The photocatalytic activity of the samples upon irradiation λ_1 (cut-off filter $\lambda > 320$ nm) is shown in Fig. 6. Dark experiments revealed that malachite green undergoes an important adsorption on TiO_2 P-25 materials impregnated with TPA, while in naked P25, this adsorption can be neglected. Under irradiation, the P25-TPA-500 sample exhibited the highest photocatalytic activity, even higher than that of Degussa P25, while the P25-TPA-200 sample showed the lowest one.

When irradiation λ_2 was used (cut-off filter $\lambda > 450$ nm) (Fig. 7), where UV light is eliminated, only the P25-TPA-500 sample showed photocatalytic activity since malachite green was almost totally degraded after 60 min of light irradiation. A decrease in MG concentration was detected for the P25-TPA-200 sample, but it was produced by dark adsorption.

Under irradiation λ_3 (filter cut-off $\lambda > 590$ nm), there was no photocatalytic bleaching of malachite green solutions (data not shown).

The effect of the addition of *tert*-butyl alcohol (TBA), an $^{\bullet}OH$ radical scavenger ($k = 6.0 \times 10^8\ M^{-1}\ s^{-1}$) [22,23], was evaluated in the photocatalytic bleaching of malachite green aqueous solutions in the presence of sample P25-TPA-500 (Fig. 8). Under irradiation λ_1 (Fig. 8a), the photocatalytic activity was slightly affected by the presence of TBA. However, under irradiation λ_2 (Fig. 8b), the photocatalytic activity did not undergo any change.

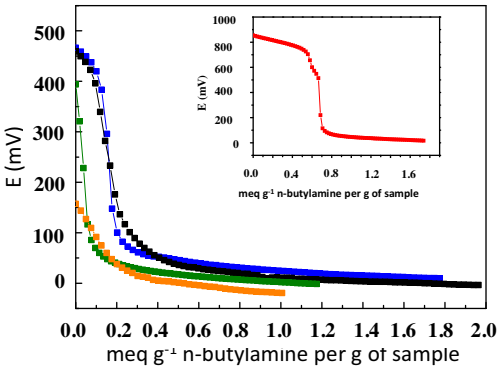

Fig. 5. Potentiometric acidity measurements of (—) P25-TPA-NA, (▬) P25-TPA-200, (▬) P25-TPA-500 and (▬) unmodified P-25. The inset shows potentiometric acidity measurements of bulk TPA.

Finally, the leaching of TPA was evaluated in the samples P25-TPA-200 and P25-TPA-500 suspended in water in the absence of MG upon irradiation λ_1 (cut-off filter at $\lambda > 320$ nm), measuring the tungsten content in aqueous media by atomic absorption spectroscopy. Analyses demonstrated that the P25-TPA-200 sample underwent a 6.0% of tungsten leaching, while the P25-TPA-500 sample exhibited only 0.046%.

4. Discussion

^{31}P MAS NMR measurements revealed that at low annealing temperatures, bulk TPA did not undergo strong changes in its

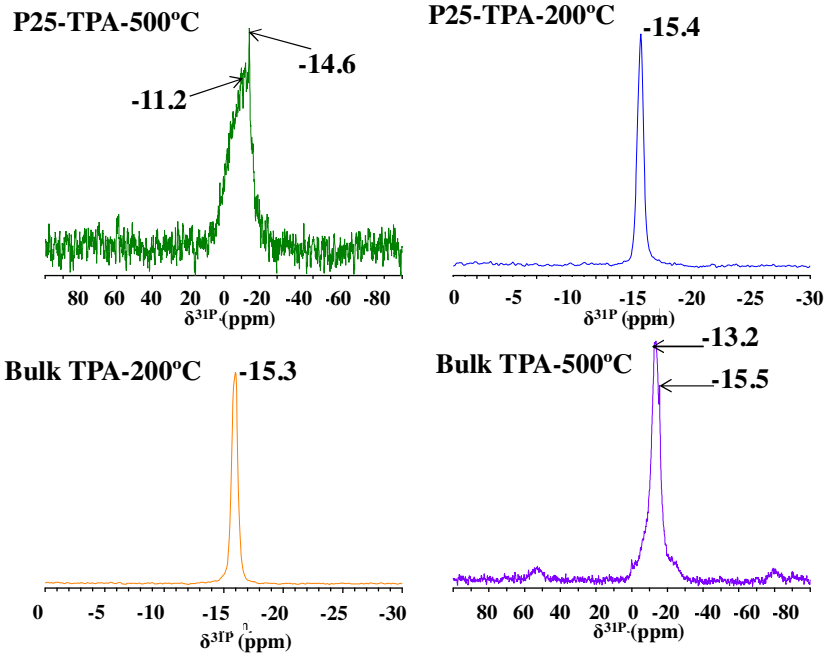

Fig. 4. ^{31}P MAS NMR spectra of P-25-TPA samples.

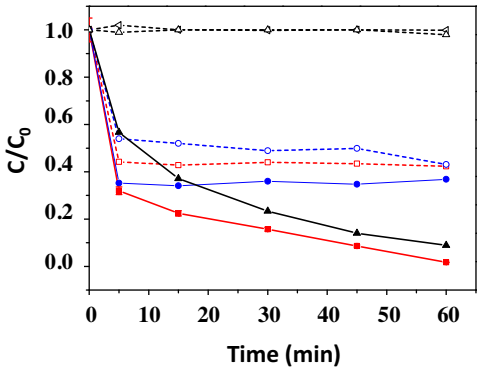

Fig. 6. Photocatalytic activity of samples upon irradiation λ_1 (cut-off filter $\lambda > 320$ nm). (-■-) P25-TPA-500, (-●-) P25-TPA-200, (-▲-) Degussa P-25, (--□--) dark adsorption on P25-TPA-500, (--○--) dark adsorption on P25-TPA-200, (--▲--) dark adsorption on Degussa P-25 and (--x--) MG + UV light. Initial pH: 5.0.

structure since only the signal at −15.3 ppm, correlated with the presence of the hydrated Keggin anion [18], was detected. Often, the ^{31}P MAS-NMR signal of TPA depends on the hydration degree and varies from −10 to −16 ppm [24]. In the spectrum of bulk TPA calcined at 500 °C, two signals appeared: one at −15.5, and the other at −13.2 ppm, which could be assigned to $PW_{12}O_{40}^{3-}$ and $HPW_{12}O_{40}^{2-}$ Keggin anions, respectively [24,25]. The broadening observed is possibly due to dehydration of the Keggin structure [26].

Regarding the samples of Evonik P25 impregnated with TPA, those annealed at 200 °C (P25-TPA-200) exhibited a narrow ^{31}P MAS-NMR signal at −15.5 ppm, which is related to the hydrated Keggin anion of TPA. However, the sample annealed at 500 °C (P25-TPA-500) exhibited a main peak at −14.6 ppm with a shoulder at −11.2 ppm, which can be attributed to the presence of Keggin anion and lacunar species ($[PW_{11}O_{39}]^{7-}$) [12,25,27], respectively, the latter coming from a partial TPA thermal degradation. The shift observed for the Keggin anion signal (from −15 to −14.6 ppm) in the sample P25-TPA-500 could be due to an interaction between the TiO_2 surface and TPA. Edwards et al. [27] have argued that signals of ^{31}P MAS NMR at −14 and −13 ppm could be due to the presence of intact Keggin units interacting with surface hydroxyl groups from TiO_2 to form species such as $(TiOH_2^+)(H_2PW_{12}O_{40}^-)$ and $(TiOH_2^+)_2(HPW_{12}O_{40}^{2-})$.

The Raman spectrum should confirm this interaction, since the main anatase Raman peak of the P25-TPA-500 sample at 141 cm^{-1} underwent a strong shift (ca. 8 cm^{-1}). Some authors have claimed that the shift of this Raman band, which arises from O—Ti—O band-bending-type vibrations, could be due to oxygen deficiencies or disorders induced by minority phases [28,29]. Moreover, the signals of TPA Keggin anion between 980 and 1020 cm^{-1} also showed a high broadening. Previous studies reported that these spectral changes could be related to strong interactions between the Keggin anion of TPA and the TiO_2 surface [13,30]. On the other hand, the interaction of TPA and the TiO_2 surface in P25-TPA-200 samples could be weaker than in the P25-TPA-500 samples since the blue shift of the Ti-O band was lower and the TPA signals between 980 and 1020 cm^{-1} did not exhibit spectral changes. Moreover, this fact could also explain the high leaching observed in the P25-TPA-200 sample, since in the P25-TPA-500 sample, TPA is probably more strongly anchored forming surface complexes than in the P25-TPA-200 sample.

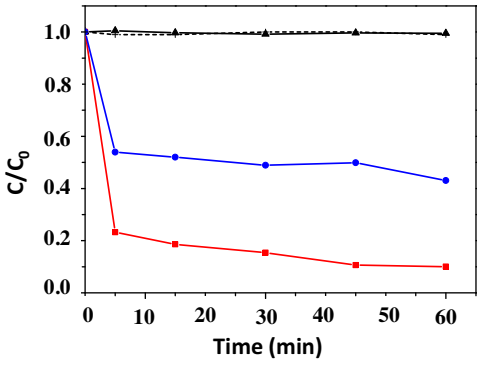

Fig. 7. Photocatalytic activity of samples upon irradiation λ_2 (cut-off filter $\lambda > 450$ nm). (-■-) P25-TPA-500, (-●-) P25-TPA-200, (-▲-) Degussa P-25, (--x--) MG + visible light. Initial pH: 5.0.

The results of potentiometric titration also showed interesting features. Either P25-TPA-NA or P25-TPA-200 samples showed a higher acid strength than P25-TPA-500. It is often accepted that TPA should interact with TiO_2 surfaces through protonation of surface Ti—OH groups by very acid protons from TPA yielding $(\equiv Ti—(OH)_2^+)(H_2PW_{12}O_{40}^-)$ or $(\equiv TiOH_2^+)_2$ $(HPW_{12}O_{40}^{2-})$ species [27,31]. This should generate acid sites on the TiO_2 surface, which should be responsible for the initial high potential (E_i) observed. However, when the sample is annealed at high temperatures (500 °C), the acid strength decreases slightly. It is suggested that this decrease could be related to the formation of surface complexes between TPA and TiO_2.

Inspired by the study reported by Legagneux et al. [32], who have proposed that at temperatures beyond 300 °C, TPA could lead to the formation of Si—O—W bonds in silica, herein it is suggested that at high temperatures (T = 500 °C), the acid proton linked to TPA in $(\equiv TiOH_2^+)_2(HPW_{12}O_{40}^{2-})$ species, which is highly reactive, could react with a protonated titanol ($TiOH_2^+$) groups, leading to water production and the formation of Ti—O—W bonds and, concomitantly, a TPA-TiO_2 surface complex, which could be responsible for the visible light absorption and spectroscopic changes observed. Keggin anion of TPA ($[PW_{12}O_{40}]^{-3}$) exhibits two intense bands in the range 200–250 nm [33], attributed to the charge transfer from bridging or terminal O 2p to W 5d (W—O—W and W—O_d). The Kegging structure consists of a central PO_4 tetrahedron surrounded by twelve WO_6 octahedra. Due to the formation of Ti—O—W bonds between Ti-OH groups and bridging or terminal O groups from the WO_6 octahedral units that conform the TPA Keggin structure, the lengths of —W—O—W or —W—O_d bonds could change leading to the distortion of the Keggin structure. Taking into account the work of Rodríguez-González et al. [34], it is suggested that visible light absorption takes place as result of this distortion.

Previous studies reported in the literature have suggested that the surface charge transfer complex formation between TiO_2 and organic or inorganic adsorbates such as phenolic compounds and EDTA could take place inducing visible light absorption [35,36].

However, not all the $(\equiv TiOH_2^+)_2(HPW_{12}O_{40}^{2-})$ and $(\equiv Ti—(OH)_2^+)(H_2PW_{12}O_{40}^-)$ species can be eliminated during the annealing step by forming surface complexes, since the P25-TPA-500 sample still exhibited an important acid strength (Fig. 9). This fact would also explain the decrease in acid strength observed in samples annealed at 500 °C.

The dark adsorption of malachite green on TPA-P25 samples could be due to a strong interaction between negatively charged nanoparticles (IP of P25-TPA-200 and P25-TPA-500 are 1.6 and 2.0, respectively) and positively charged dye molecules. On the other hand, a previous study reported the interaction between malachite green molecules and TPA through electrostatic interactions [37].

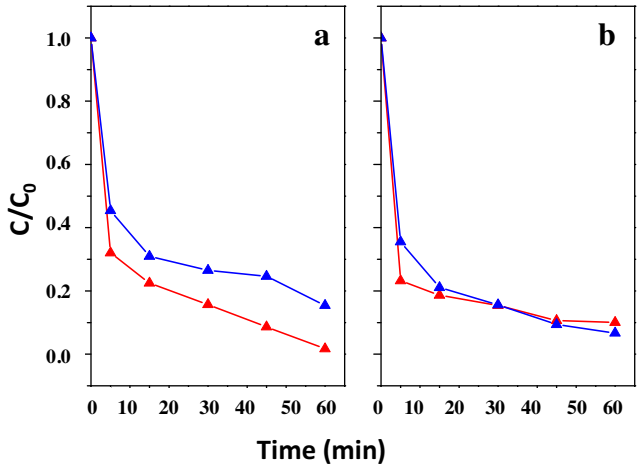

Fig. 8. Photocatalytic activity of the P25-TPA-500 sample upon (a) irradiation λ_1 (cut-off filter $\lambda > 320$ nm) (b) irradiation λ_2 (cut-off filter $\lambda > 450$ nm) in the absence (- ▲ -) and in the presence (- ▲ -) of *tert*-butyl alcohol (TBA). Initial pH: 5.0.

Photocatalytic activity under irradiation λ_1, which contains UV-A light, revealed that the P25-TPA-500 sample exhibited the highest photocatalytic activity. This fact is explained since the TPA present on the TiO_2 surface may behave like an efficient electron acceptor since its redox potential is more positive ($E_{TPA} = -0.01$ V vs E_{eCB} (pH 5) $= -0.27$ V) than the redox potential of the conduction band electron (E_{eCB}) [33,38]. Thus, the UV-photo-excited electron transfer from the conduction band of TiO_2 to TPA should be thermodynamically favoured, decreasing the e^-/h^+ recombination. Experiments using *tert*-butyl alcohol as $^\bullet$OH radical scavenger also revealed that malachite green oxidation could be carried out by h^+ and/or $^\bullet$OH radicals since a decrease in the photocatalytic activity took place when 1×10^{-5} M of TBA was added. Thus, it is possible to suggest that the mechanism of malachite green oxidation by P25-TPA-500 may involve the excitation of electrons from the valence band to the conduction band. These photo-promoted electrons could be easily transferred to the Keggin anion of TPA present either as a surface complex or as ($\equiv$Ti—$(OH)_2^+$)($H_2PW_{12}O_{40}^-$) or ($\equiv TiOH_2^+)_2$ ($HPW_{12}O_{40}^{2-}$) species on the TiO_2 surface (Fig. 9). Thus, the e^-/h^+ recombination would decrease, leaving more h^+ available in the valence band of TiO_2 to react either with previously adsorbed malachite green molecules or H_2O molecules, the latter leading to $^\bullet$OH radical production. Under irradiation λ_2, which contains visible irradiation able to excite the visible-light-absorbing P25-TPA-500 sample and the malachite green molecule ($\lambda_{max} = 618$ nm), one more time, sample P25-TPA-500 showed the best photocatalytic activity. Moreover, experiments using *tert*-butyl alcohol did not reveal a negative effect on the photocatalytic activity. The suggested mechanism to explain these results seems to be more complicated. It is well known that photo-excited POMs such as TPA can lead to the oxidation of organic compounds by electron transfer, resulting in its reduction through photosensitized reactions. This oxidation is favoured when the organic molecule is preassociated with the POM [33] (Fig. 10).

The visible-light-absorbing surface complex of TPA Keggin anion with TiO_2 could participate in the observed malachite green oxidation. Malachite green, which was previously interacting with TPA species on TiO_2 (strong dark adsorption), could be directly oxidized by the visible-light-excited TPA-TiO_2 surface complex, since the excited state of redox molecules is both a better oxidant and better reductant than the ground state, producing a photosensitized reaction. Reduced TPA (TPA^-) could be re-oxidized taking into account that POM tungstates are easily re-oxidized by oxygen (Fig. 11a) [33].

Another mechanism (Fig. 11b) that could be involved in the photocatalytic activity observed may lead to the electron transfer from the TPA excited state (TPA*) to the conduction band of TiO_2. This electron may be able to reduce molecular oxygen previously adsorbed on the TiO_2 surface, leading to the generation of H_2O_2, which could also be reduced by CB electrons yielding $^\bullet$OH radicals

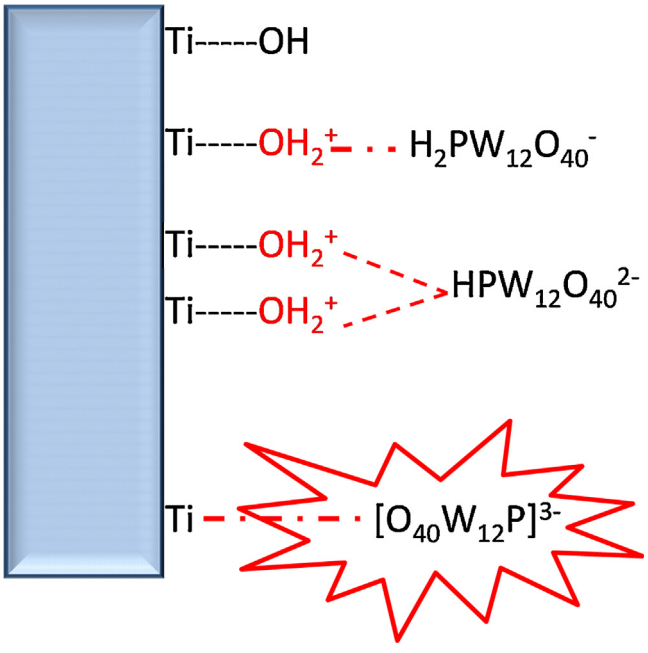

Fig. 9. Possible TPA-TiO_2 surface interactions.

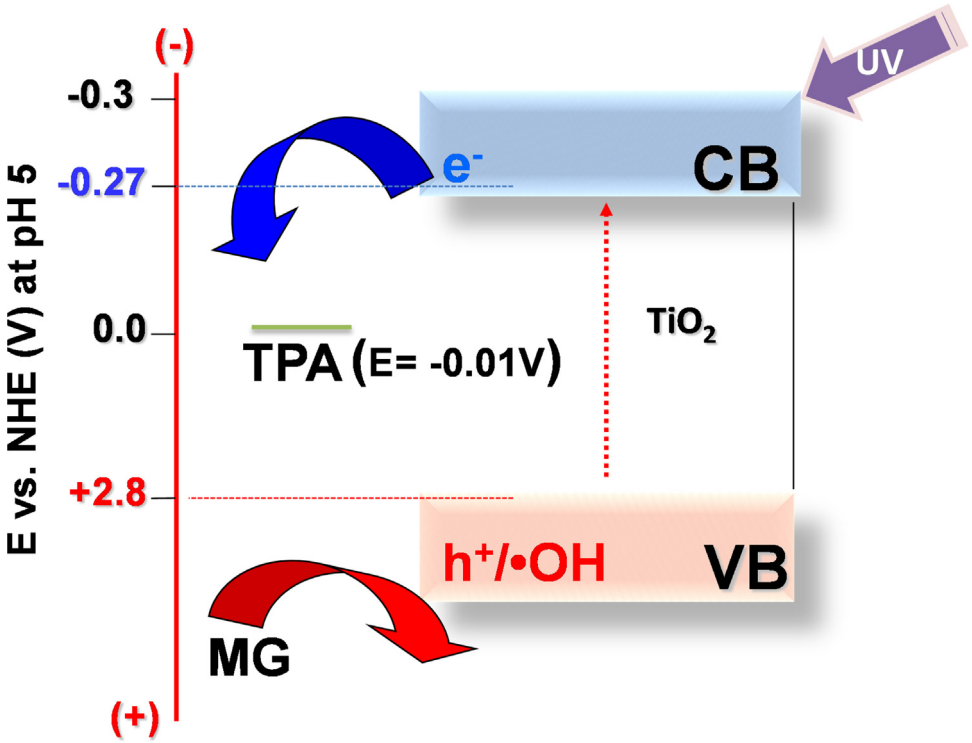

Fig. 10. Photocatalytic mechanism suggested for MG degradation on P25-TPA-500 samples upon UV irradiation.

that may oxidize the dye molecules. The oxidized TPA^+ species could be reduced by malachite green molecules, leading to dye oxidation and the regeneration of TPA. This should explain the small reduction of the photocatalytic activity in the presence of TBA.

Finally, in order to discard the participation of MG molecules (involving MG excited states) in the photosensitized reactions that would be responsible for dye solution photobleaching, experiments carried out under irradiation λ_3, which could only produce excitation of MG, revealed that dye oxidation does not involve photochemical reactions of MG excited states.

5. Conclusions

It is concluded that Evonik P-25 TiO_2 powders containing 30% (w/w) of tungstophosphoric acid (TPA) and annealed at 500 °C exhibited visible light absorption and high photocatalytic activity upon UV (λ_1) and visible light irradiation (λ_2). At high temperatures (ca. 500 °C), the Keggin anion of TPA should interact with the TiO_2 surface by forming TPA-TiO_2 complexes and two kinds of electrostatic species: $(\equiv Ti{-}(OH)_2^+)(H_2PW_{12}O_{40}^-)$ or $(\equiv TiOH_2^+)_2$ $(HPW_{12}O_{40}^{2-})$. The former should be responsible for visible light absorption and FT-Raman and ^{31}P MAS NMR spectral changes and the latter, for the high acid strength and low IP observed. At low annealing temperatures (200 °C), P25-TPA materials did not exhibit visible light absorption but high acid strength, revealing that temperature played an important role in the interaction between TPA Keggin anion and the TiO_2 surface. Samples annealed at 500 °C exhibited lower tungsten (W) leaching than those annealed at 200 °C.

Malachite green (MG) molecules underwent strong dark adsorption on the surface of TPA-impregnated TiO_2 P-25 samples (P25-TPA-200 and P25-TPA-500). This should be due to the fact that at pH 5.0 (at which the photocatalytic experiments were performed), TPA-impregnated TiO_2 P-25 samples are negatively charged (the isoelectric points of P25-TPA-200 and P25-TPA-500 are 1.4 and 2.0, respectively), allowing an electrostatic interaction with cationic malachite green molecules. Upon UV irradiation (λ_1), complexed or noncomplexed TPA in P25-TPA-500 sample should be responsible for the high photocatalytic activity, since the polyoxometallate should act as a sink of photoinduced conduction band electrons, decreasing the e^-/h^+ recombination and leaving more valence band holes available to either directly oxidize malachite green molecules or produce •OH radicals by water oxidation. Furthermore, the sample annealed at 500 °C showed the highest photocatalytic activity, even higher than that of the unmodified Evonik P-25 sample. The photocatalytic activity of P25-TPA-500 sample was affected by the addition of *tert*-butyl alcohol (TBA), an •OH scavenger, evidencing the participation of photoinduced valence band holes (h^+) and/or •OH radicals in the degradation of MG.

Upon visible light irradiation (λ_2), P25-TPA-500 sample was the only one that showed an interesting photocatalytic activity. This correlated well with the ability of this sample to absorb visible light. However, the presence of TBA slightly affected its photocatalytic activity, suggesting that the photocatalytic mechanism should be different. Indeed complexed TPA on the TiO_2 surface should be responsible for this photocatalytic activity, since photosensitized reactions involving excited states of the TPA-TiO_2 complex could directly oxidize the MG molecules or could also inject electrons into the TiO_2 conduction band, leading to the indirect formation of •OH radicals.

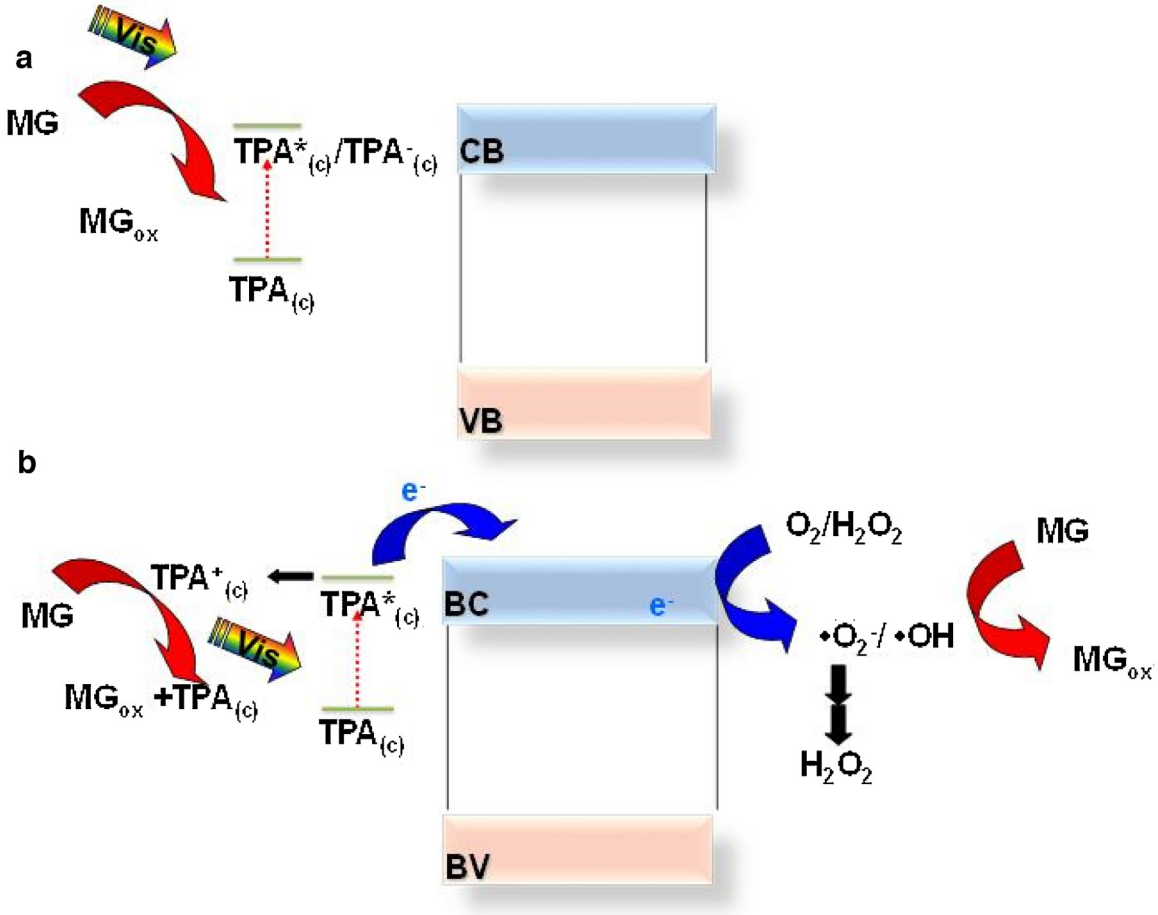

Fig. 11. Photocatalytic mechanism suggested for MG degradation on P25-TPA-500 samples upon visible irradiation.

Acknowledgements

Authors thank the financial support from CONICET (PIP 628) and Universidad Nacional de La Plata (UNLP) (Project number X638) and the technical assistance of Mariela Theiller in the SEM/EDX analysis and Lilian Osiglio in the potentiometric titrations.

Appendix A. Supplementary data

Supplementary data associated with this article can be found, in the online version, at http://dx.doi.org/10.1016/j.materresbull.2016.06.026.

References

[1] R.I. Bickley, T. Gonzales-Carreno, J.S. Lees, L. Palmisano, R.J.D. Tilley, J. Solid State Chem. 92 (1991) 178.
[2] D.C. Hurum, D.G. Agrios, K.A. Gray, T. Rajh, M.C. Thurnauer, J. Phys. Chem. B. 107 (2003) 4545.
[3] I.E. Saliby, L. Erdei, H.K. Shon, J.H. Kim, J. Ind. Eng. Chem. 17 (2011) 358.
[4] W. Yan, Z. Jiwei, J. Zhen Shen, W. Zhinshen, Z. Shunli, Chin. Sci. Bull. 52 (2007) 2157.
[5] X. Fang, Z. Quinglin Chen, H. Ji, X. Gao, J. Solid State Chem. 180 (2007) 1325.
[6] J.A. Rengifo-Herrera, J. Kiwi, C. Pulgarin, J. Photoch. Photobiol. A-Chem. 205 (2009) 109.
[7] P.A. Osorio-Vargas, C. Pulgarin, A. Sienkiewicz, L.R. Pizzio, M.N. Blanco, R.A. Torres-Palma, C. Petrier, J.A. Rengifo-Herrera, Ultrason. Sonochem. 19 (2012) 383.
[8] C. Yu, J.C. Yu, W. Zhou, K. Yang, Catal. Lett. 140 (2010) 172.
[9] N. Lu, Y. Zhao, H. Liu, Y. Guo, X. Yuan, H. Xu, H. Peng, H. Quin, J. Hazard. Mater. 199-200 (2012) 1.
[10] R. Sivakumar, J. Thomas, M. Yoon, J. Photoch. Photobiol. C-Rev. 13 (2012) 277.
[11] S.S. Wang, G.Y. Yang, Chem. Rev. 115 (2015) 4893.
[12] J.A. Rengifo-Herrera, M.N. Blanco, L.R. Pizzio, Appl. Catal. B-Env. 110 (2011) 126.
[13] J.A. Rengifo-Herrera, M.N. Blanco, L.R. Pizzio, Mater. Res. Bull. 49 (2014) 618.
[14] T. Ohno, K. Sarukawa, K. Tokieda, M. Matsumura, J. Catal. 203 (2001) 82.
[15] I. Holclajtner-Antunovic, D. Bajuc-Bogdanovic, A. Popa, U.B.S. Uskokovic-Markovic, Inorg. Chim. Acta. 383 (2012) 26.
[16] I. Holclajtner-Antunovic, U.B. Mioc, M. Todorovic, Z. Jovanovic, M. Davidovic, D. Bajuc-Bogdanovic, Z. Lausevic, Mater. Res. Bull. 45 (2010) 1679.
[17] Y. Cong, J. Zhang, F. Chen, M. Anpo, J. Phys. Chem. C. 111 (2007) 6976.
[18] F. Lefebvre, J. Chem. Soc. Chem. Commun. 10 (1992) 756.
[19] R. Cid, G. Pecci, Appl. Catal. 14 (1985) 15.
[20] L.R. Pizzio, M.N. Blanco, Appl. Catal. A-Gen. 255 (2003) 265.
[21] U. Diebold, Surf. Sci. Rep. 48 (2003) 53.
[22] J. Staehelin, J. Hoigne, Environ. Sci. Technol. 19 (1985) 1206.
[23] S. Enami, Y. Sakamoto, A.J. Colussi, Proc. Natl. Acad. Sci. U. S. A. 111 (2014) 623.
[24] E. Caliman, J.A. Dias, S.C.L. Dias, A.G.S. Prado, Catal. Today. 107–108 (2005) 816.
[25] T. Okuhara, N. Mizuno, M. Misono, Adv. Catal. 41 (1996) 113.
[26] N. Essayem, Y.Y. Tong, H. Jabic, J.C. Vedrine, Appl. Catal. A-Gen. 194–195 (2000) 109.
[27] J.C. Edwards, C.Y. Thiel, B. Benac, J.F. Knifton, Catal. Lett. 51 (1998) 77.
[28] M. Pelaez, P. Falaras, V. Likadimos, A.G. Kontos, A.A. De la Cruz, K. O'shea, D. Dyonysiou, Appl. Catal. B-Env. 99 (2010) 378.
[29] G. Colon, M.C. Hidalgo, J.A. Navío, A. Kubacka, M. Fernández-García, Appl. Catal. B-Env. 90 (2009) 633.
[30] L. Li, Q.-Y. Wu, Y.-H. Guo, C.-W. Hu, Mater. Res. Soc. 87 (2005) 1.
[31] Y. Yang, Q. Wu, Y. Guo, C. Hu, E. Wang, J. Mol. Catal. A-Chem. 225 (2005) 203.
[32] N. Legagneux, J.-M. Basset, A. Thomas, F. Lefebvre, A. Goguet, J. Sá, C. Hardacre, Dalton Trans. 12 (2009) 2235.
[33] E. Papaconstantinou, Chem. Soc. Rev. 18 (1989) 1.
[34] V. Rodríguez-González, E. Marceau, M. Che, C. Pepe, J. Solid State. Chem. 180 (2007) 3469.
[35] J.C. Parker, R.W. Siegel, Appl. Phys. Lett. 57 (1990) 943.
[36] S. Kim, W. Choi, J. Phys. Chem. B. 109 (2005) 5143.
[37] Y. Song, S. Liu, Z. Liu, X. Hu, Spectrochim. Acta A. 78 (2011) 148.
[38] A. Fujishima, X. Zhang, D.A. Tryk, Surf. Sci. Rep. 68 (2008) 515.